

Simulation-based Inference for Model Parameterization on Analog Neuromorphic Hardware

Jakob Kaiser^{a,2}, Raphael Stock^a, Eric Müller^b, Johannes Schemmel^{a,2}, and Sebastian Schmitt^c

^aKirchhoff-Institute for Physics, Heidelberg University, 69120 Heidelberg, Germany

^bEuropean Institute for Neuromorphic Computing, Heidelberg University, 69120 Heidelberg, Germany

^cDepartment for Neuro- and Sensory Physiology, University Medical Center Göttingen, 37077 Göttingen, Germany

²Corresponding authors (jakob.kaiser@kip.uni-heidelberg.de or schemmel@kip.uni-heidelberg.de)

February 20, 2024

The BrainScaleS-2 (BSS-2) system implements physical models of neurons as well as synapses and aims for an energy-efficient and fast emulation of biological neurons. When replicating neuroscientific experiment results, a major challenge is finding suitable model parameters. This study investigates the suitability of the sequential neural posterior estimation (SNPE) algorithm for parameterizing a multi-compartmental neuron model emulated on the BSS-2 analog neuromorphic hardware system. In contrast to other optimization methods such as genetic algorithms or stochastic searches, the SNPE algorithm belongs to the class of approximate Bayesian computing (ABC) methods and estimates the posterior distribution of the model parameters; access to the posterior allows classifying the confidence in parameter estimations and unveiling correlation between model parameters. In previous applications, the SNPE algorithm showed a higher computational efficiency than traditional ABC methods.

For our multi-compartmental model, we show that the approximated posterior is in agreement with experimental observations and that the identified correlation between parameters is in agreement with theoretical expectations. Furthermore, we show that the algorithm can deal with high-dimensional observations and parameter spaces.

These results suggest that the SNPE algorithm is a promising approach for automating the parameterization of complex models, especially when dealing with characteristic properties of analog neuromorphic substrates, such as trial-to-trial variations or limited parameter ranges.

Keywords: analog | neuromorphic | simulation-based inference | multi-compartment

1 Introduction

Mechanistic models, which try to explain the causality between inputs and outputs, are integral to scientific research. On the one hand they can increase the understanding of the mechanisms which cause the phenomena and on the other make predictions about new outcomes which can then be tested experimentally (Baker et al., 2018). After a mechanistic model has been formulated, one of the remaining challenges is to find suitable model parameters which lead to a close agreement between the model behavior and the experimental observation.

Several approaches such as the hand-tuning of parameters,

grid searches, random/stochastic search, evolutionary algorithms, simulated annealing and particle swarm algorithms have been used in neuroscience to find appropriate model parameters (Vanier and Bower, 1999; Van Geit et al., 2008). Drawbacks of these methods are that they rely on a score which represents how close the results of a simulated model are to the target observation and that they in general only yield the best performing set of parameters. Furthermore, these algorithms are often computationally expensive since they require many simulations to find suitable parameters (Gonçalves et al., 2020).

The class of ABC algorithms makes statistical inference methods available for models where the likelihood is not tractable and allows finding an approximation of the posterior distribution of the model parameters. Advantages of deriving an approximation of the posterior include the possibility to find correlations between model parameters and to classify the confidence in the estimated parameters. Early approaches to ABC rely on defining a score and are computationally inefficient since they disregard many simulation results if their score is too low (Sisson et al., 2018).

Recent advances in machine learning lead to a new class of likelihood-free inference (LFI) algorithms (also called simulation-based inference (SBI) algorithms) which promise to be computationally more efficient and do not depend on a score function (Papamakarios and Murray, 2016; Lueckmann et al., 2017; Greenberg et al., 2019; Cranmer et al., 2020; Deistler et al., 2022). In this paper we will focus on the SNPE algorithm which was already applied to infer parameters for different neuroscientific models (Lueckmann et al., 2017; Gonçalves et al., 2020). More specifically, we want to investigate if this algorithm is suitable to parameterize neuron models which are emulated on the BSS-2 analog neuromorphic hardware (Pehle et al., 2022).

Neuromorphic computation draws inspiration from the brain to find time and energy-efficient computing architectures as well as algorithms (Indiveri et al., 2011). The BSS-2 system emulates the behavior of neurons and synapses on analog neurons in continuous time (Billaudelle et al., 2022) and does not solve the model equations mathematically like digital neuromorphic hardware (Davies et al., 2018; Furber et al., 2012; Mayr et al., 2019).

In previous experiments on the BSS-2 system, hardware parameters were set by calibration routines, grid searches, gradient-based optimization or by hand-tuning (Billaudelle et al., 2022; Aamir et al., 2018; Wunderlich et al., 2019; Kaiser et al., 2022). The hand-tuning of parameters can be tedious and relies on the domain-specific knowledge of the experimenter

such that automated parameter-search methods are inevitable for complex problems (Vanier and Bower, 1999). Similarly, a calibration routine can only be formulated if the relationship between the parameters and their impact on the observation is known. Depending on the dimensionality of the parameter space, grid searches and random searches can be computationally too expensive. The SNPE algorithm promises to find approximations of the posterior even if the parameter space is high-dimensional and the relationship between the parameters and the observation is unknown.

Furthermore, the SNPE algorithm is designed for probabilistic models. This makes it a suitable choice for models which deal with intrinsic probabilistic behavior such as analog neuro-morphic hardware which is subject to temporal noise.

1.1 BrainScaleS-2

BSS-2 is a neuromorphic system which emulates the behavior of neuron and synapse with the help of analog circuits. 512 neuron circuits are able to replicate the dynamics of the adaptive exponential integrate-and-fire (AdEx) neuron model (Brette and Gerstner, 2005); adaptation and exponential term can be switched off to obtain the dynamics of the simpler leaky integrate-and-fire (LIF) model (Billaudelle et al., 2022). Furthermore, neuron circuits can be connected via adjustable resistances to implement multi-compartmental neuron models with different morphologies (Kaiser et al., 2022). In this publication, we will consider multi-compartmental neuron models for which the membrane potentials in the different compartments V_m adhere to the dynamics of the LIF neuron model,

$$C_m \frac{dV_m(t)}{dt} = g_{\text{leak}} \cdot (V_{\text{leak}} - V_m(t)) + I_{\text{syn}}(t) + I_{\text{axial}}(t), \quad (1)$$

where C_m is the membrane capacitance, g_{leak} the leak conductance and V_{leak} the leak potential.

The two currents in Equation (1) arise due to synaptic input, I_{syn} , and connections to neighboring compartments, I_{axial} . The synaptic current I_{syn} models current-based synapses with an exponential kernel. The current $I_{\text{axial},i}(t)$ on compartment i ¹ due to neighboring compartments is given by

$$I_{\text{axial},i}(t) = \sum_j g_{\text{axial}}^{i \leftrightarrow j} \cdot (V_{m,j}(t) - V_{m,i}(t)), \quad (2)$$

where the sum runs over all neighboring compartments $\{j\}$, $g_{\text{axial}}^{i \leftrightarrow j}$ represents the conductance between these compartments and V_j the membrane potential of the neighboring compartment.

Once the membrane potential V_m crosses a threshold potential V_{thres} a spike is generated and the membrane potential is reset to the reset potential V_{reset} .² After the refractory time τ_{ref} the reset is released and the membrane potential V_m continues to adhere to the dynamics of Equation (1).

The parameters of each neuron can be set individually. Digital parameters control which terms of the AdEx model are enabled while analog reference currents and voltages control parameters such as leak potential and leak conductance. The analog references are provided by an analog on-chip memory array which converts digital 10 bit values to currents and voltages (Hock et al., 2013). This high degree of configurability allows tuning the neuron circuits to a variety of different operating regimes (Billaudelle et al., 2022) and to compensate manufacturing-induced mismatch between different neuron circuits.

¹Since all variables in Equation (1) refer to compartment i , we omitted the subscript i in Equation (1) for easier readability.

²These digital spikes can be used as an input for other neurons on the chip or can be recorded as an observable

1.2 Sequential Neural Posterior Estimation Algorithm

The SNPE algorithm (Papamakarios and Murray, 2016; Lueckmann et al., 2017; Greenberg et al., 2019) belongs to the class of LFI algorithms and allows finding an approximation of the posterior distribution $p(\theta | \mathbf{x}^*)$ in cases where the likelihood $p(\mathbf{x} | \theta)$ is intractable. Here θ are the parameters of a mechanistic model for which we try to find parameters which reproduce a target observation \mathbf{x}^* . The main idea is to evaluate the model for different parameters $\{\theta_i\}$, extract the observations $\{\mathbf{x}_i\}$ and fit a flexible probability distribution as a posterior to this set of parameters and observations. As the name suggests the parameters of these probability distributions are determined by neural networks.

Similar as for traditional ABC methods a target observation \mathbf{x}^* , prior $p(\theta)$ and a model for which suitable parameters should be found are provided as an input to the algorithm, Figure 1B. The prior is used to draw random parameters $\theta' \sim p(\theta)$. By evaluating the model with the given parameters θ' we implicitly sample from the likelihood $\mathbf{x}' \sim p(\mathbf{x} | \theta')$. In our case the evaluation of the model is the emulation on the BSS-2 system.

In the second step, a neural density estimator (NDE) is trained to approximate the posterior distribution $p(\theta | \mathbf{x})$. The NDE is a flexible set of probability distributions which are parameterized by a neural network. Typical choices are mixed-density networks (Papamakarios and Murray, 2016; Lueckmann et al., 2017; Greenberg et al., 2019) or masked autoregressive flows (MAFs) (Goncalves et al., 2020; Papamakarios et al., 2021). The NDE is commonly trained by minimizing the negative log-likelihood of the previously drawn parameters and samples. Therefore, unlike traditional ABC algorithms the SNPE algorithm does not depend on a user-defined score function. After training, the NDE approximates the posterior distribution of the parameters for any observation \mathbf{x} .

If we are only interested in a single target observation \mathbf{x}^* , we can use the estimated posterior distribution in the following rounds as a proposal prior (Papamakarios and Murray, 2016). While this sequential approach can increase sample efficiency, the obtained approximation of the posterior is no longer amortized, i.e. it can only be used to infer parameters for the target observation \mathbf{x}^* and not any arbitrary observation \mathbf{x} .

2 Results

In order to test the capabilities of the SNPE algorithm, we consider a multi-compartmental model which consists of a chain of passive compartments, see Figure 2. Such multi-compartmental models have been used to model dendrites and axons (Rall, 1962; Fatt and Katz, 1951). Each compartment i is connected to a leak potential V_{leak} via a leak conductance g_{leak}^i and to the neighboring compartment via an axial conductance $g_{\text{axial}}^{i \leftrightarrow i+1}$, compare Equation (2). These conductances serve as our parameters θ , all other parameters are fixed.

We inject synaptic inputs in the different compartments and observe how the post-synaptic potentials (PSPs) propagate along the chain, Figure 2. Since we are only interested in the passive propagation, we disable the spiking threshold, this is equivalent to $V_{\text{thres}} \rightarrow \infty$. Due to the low-pass properties of the passive chain, the response in the first compartment broadens and its height decreases as the synaptic input is injected more distal from the first compartment, compare first row in Figure 2. A similar behavior is visible when we look at the voltage traces in the second compartment: the PSPs broaden and flatten for more distal inputs. Since we consider a finite chain, we can also see that an input at the end of the chain affects the membrane potential more strongly, for example $h_{10} > h_{12}$.

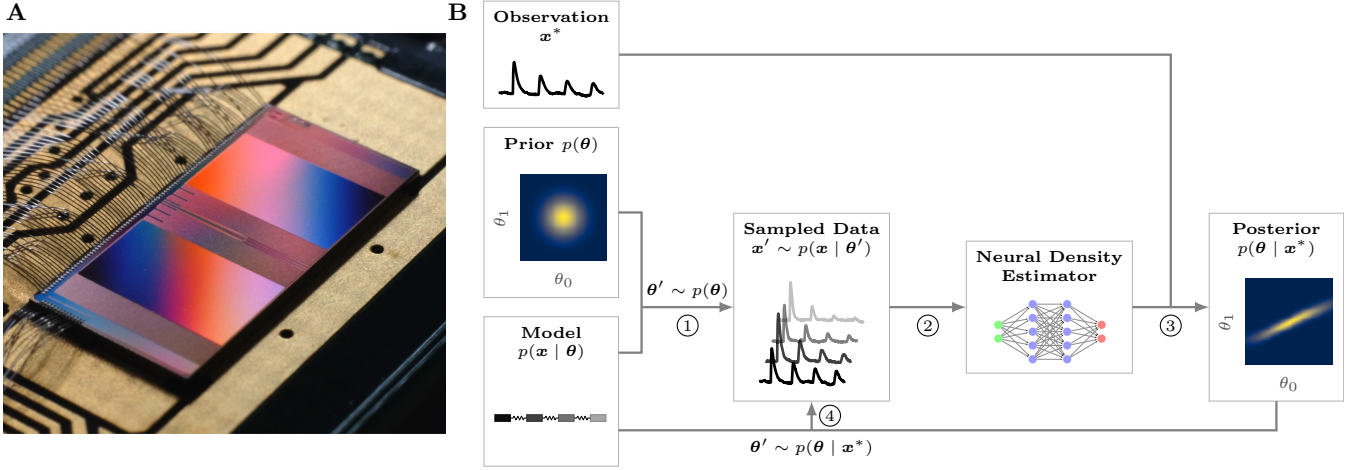


Figure 1: The BrainScaleS-2 (BSS-2) system and the sequential neural posterior estimation (SNPE) algorithm. **A** Photograph of the BSS-2 neuromorphic chip bonded to a carrier board. **B** Visualization of the SNPE algorithm (Papamakarios and Murray, 2016; Lueckmann et al., 2017; Greenberg et al., 2019). This algorithm can be used to find an approximation for the posterior distribution $p(\theta | \mathbf{x}^*)$ of parameters θ which recreate a target observation \mathbf{x}^* . The target observation \mathbf{x}^* , a prior belief about the parameter distribution $p(\theta)$ and a model which gives implicit access to the likelihood $p(\mathbf{x} | \theta)$ are given as inputs to the algorithm. In step ①, we sample parameters θ' from the prior distribution and the model is evaluated with these parameters to obtain observations \mathbf{x}' . This implicitly allows us to sample from the likelihood $p(\mathbf{x} | \theta')$. In the following step ②, the set of parameters and the corresponding observations are used to train a neural density estimator (NDE). The NDE serves as a surrogate for the posterior distribution $p(\theta | \mathbf{x})$. In general, we are interested in a single observation \mathbf{x}^* and we can restrict the NDE to this observation, step ③. We can now use samples drawn from the posterior $\theta' \sim p(\theta | \mathbf{x}^*)$ to generate new samples and retrain the NDE, repeating step ② and ③. Steps ② to ④ can be repeated several times to improve the estimate of the posterior. The figure is based on (Gonçalves et al., 2020, Figure 1).

The height of the PSPs depends on the leak and axial conductance (Fatt and Katz, 1951). If we look at the response at the injection site, a higher leak or axial conductance will result in lower heights as less charge can accumulate in the compartment. Therefore, the PSP heights \mathbf{H} or quantities derived from them are suitable observations \mathbf{x} that can be used to infer parameters θ .

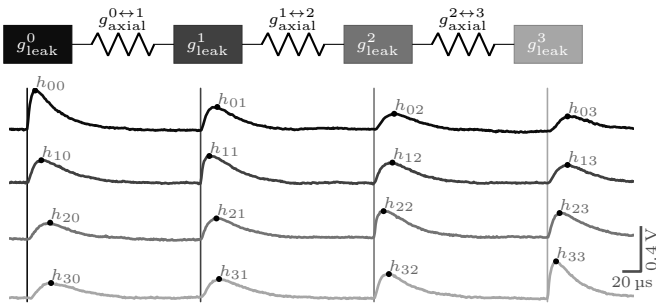


Figure 2: Model of a passive compartment chain. The parameters of the model are given by the leak conductance in each compartment g_{leak}^i and the axial conductance between compartments g_{axial}^{i+1} . In our experiment we observe the propagation of post-synaptic potentials (PSPs). Here we show membrane traces of neurons which were emulated on the BrainScaleS-2 system. We inject a synaptic input (vertical lines) in one compartment after another and record the membrane potential in each compartment (different rows). From these traces we extract the height of the PSP h_{ij} . We use the matrix of all heights \mathbf{H} , the heights resulting from an input to the first compartment $\mathbf{F} = [h_{00}, h_{10}, h_{20}, h_{30}]$ or the decay constant τ from an exponential fit to \mathbf{F} as observables. The scale bar in the lower right corner indicates the voltage and time in the hardware domain.

2.1 Two-dimensional Parameter Space

Before looking at a higher-dimensional parameter space in the next section, we reduce the dimensions of the parameter space to two by setting the leak and axial conductance for all compartments and connections to the same digital value³; $g_{\text{leak}}^i = g_{\text{leak}} \forall i \in \{0, 1, 2, 3\}$ and $g_{\text{axial}}^{i+1} = g_{\text{axial}} \forall i \in \{0, 1, 2\}$. This allows us to easily visualize and analyze the approximated posteriors. Furthermore, the low-dimensional parameter space allows us to perform a grid search in a reasonable amount of time. The grid search result can give an intuition about the behavior of the chain and can be used as a comparison to the approximated posterior obtained with the SNPE algorithm.

2.1.1 Grid Search

In order to obtain an overview of the model behavior, we perform a grid search over the two-dimensional parameter space. We create a grid of parameters by choosing equally spaced values of the leak conductance and the axial conductance which span the whole parameter range. The model is then emulated with these parameters on the BSS-2 system and the membrane traces in the different compartments are recorded. In order to easily visualize the results, we choose a one-dimensional observable. Exponential fits to the maximal height of propagating PSPs were used in other publications to classify the attenuation of PSPs in apical dendrites (Berger et al., 2001). Similarly, we fit an exponential to the PSP heights which result from an

³Due to the production induced mismatch between analog circuits, the same digital values lead to different conductances on the BSS-2 system.

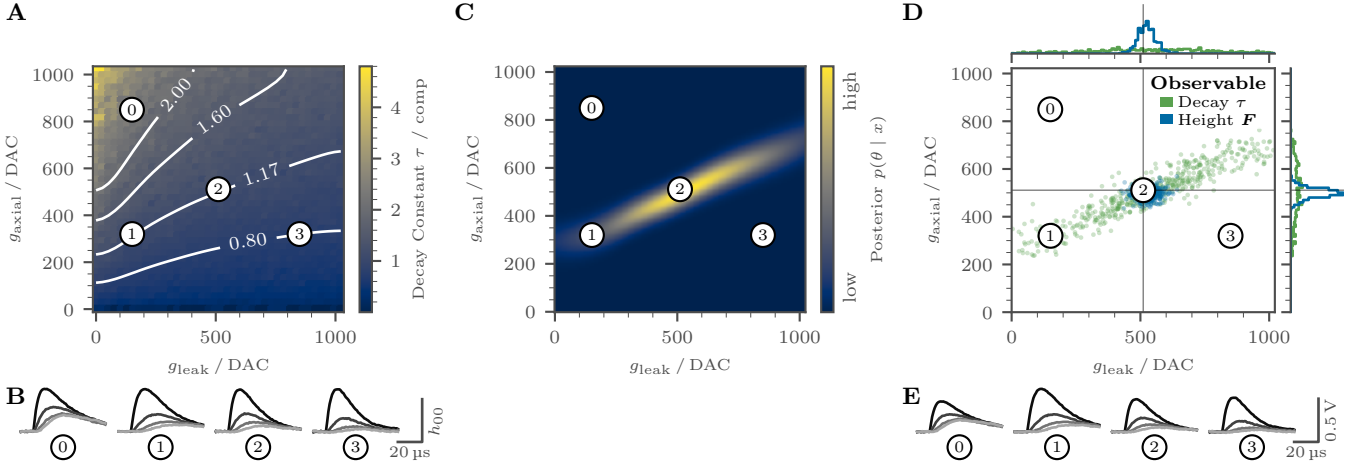


Figure 3: Propagation of post-synaptic potentials (PSPs) in a passive chain of four compartments emulated on the BrainScaleS-2 system. Leak and axial conductance are set to the same value for all compartments and connections between compartments. **A** Grid search of the decay constant τ ; the decay constant is given in units of “compartments” and calculated by fitting an exponential to the post-synaptic potentials which result from an input to the first compartment, compare Figure 2. We divided the parameter space in an evenly spaced grid with 40 values in each dimension and recorded the resulting PSP heights in each compartment, compare Figure 2. Next, we fitted an exponential decay to the PSP which resulted from an input to the first compartment and extracted the decay constant τ , Figure 5 shows the exponential fits for some exemplary measurements. The decay constant τ decreases as the leak conductance g_{leak} is increased or the axial conductance g_{axial} is reduced. The white contour lines mark regions with equal decay constant and show a correlation between leak and axial conductance. Traces recorded at the numbered points are displayed in panel B and E. **B** Example traces recorded at different locations in the parameter space, compare panel A. The traces are scaled relative to the height in the first compartment h_{00} . Due to the faster emulation of the neural dynamics on BSS-2, the time scales are in the microsecond rather than in the millisecond range. **C** Posterior obtained with the sequential neural posterior estimation algorithm. The posterior shows a high density in the parameter region where the target decay constant τ^* was recorded, ②. As expected from the grid search result in panel A, we also see a correlation between the leak and axial conductance. Points where the decay constant is significantly lower/higher than the target observation show a low probability density, ① and ③. **D** 500 random samples drawn from the approximated posteriors for two different types of observations. The green points represent samples drawn from the posterior which is shown in panel C. The samples show a correlation between both parameters. If the absolute heights of the PSP which result from an input to the first compartment $\mathbf{F} = [h_{00}, h_{10}, h_{20}, h_{30}]$ are chosen as observations (blue), the samples scatter around point ② where the original target \mathbf{F}^* was recorded. The histograms at the top and right of the scatter plot show histograms of the parameter distribution in one dimension. **E** Same traces as in panel B but shown on an absolute scale. While traces ① and ② share a similar decay constant τ , compare panel A and B, their absolute height differs.

input to the first compartment $\mathbf{F} = [h_{00}, h_{10}, h_{20}, h_{30}]$ and analyze the exponential decay constant τ , Figure 3A. The decay constant increases with increasing axial conductance g_{axial} and decreasing leak conductance g_{leak} . Even though the exponential is just an approximation for the attenuation of transient inputs in multi-compartmental models, a correlation between leak and axial conductance is expected (Fatt and Katz, 1951; Rall, 1962).

The responses of the membrane potentials to a synaptic input in the first compartment are displayed in Figure 3B. For a low leak and a large axial conductance ①, the attenuation is the weakest and the PSP is still clearly visible in the last compartment. Parameters on the same contour line show as expected similar attenuation, ① and ②, even though the exact shape of the PSPs differ. For a large leak and a low axial conductance, ③, the PSP decays quickly and is already near zero in the third compartment.

2.1.2 Simulation Based Inference

We will now use the SNPE algorithm to infer possible parameters $\theta = [g_{\text{leak}}, g_{\text{axial}}]$ which reproduce a target observation $\mathbf{x}^* = [\tau^*]$. Furthermore, we will investigate how the posterior distribution changes when we use a more informative observation $\mathbf{x}^* = \mathbf{F}^* = [h_{00}^*, h_{10}^*, h_{20}^*, h_{30}^*]$, compare Figure 2.

In the case where a target observation \mathbf{x}^* is given by an experiment, the true posterior and the optimal parameters which replicate the observation are typically unknown. This makes it hard to assess the quality of the approximated posterior found with the SNPE algorithm. Therefore, we will explicitly choose target parameters θ^* , emulate our model with these parameters on BSS-2 and measure an “artificial” target observation $\mathbf{x}^* = \tau^*$. This allows us to perform a closure test and check whether the SNPE algorithm is able to estimate a posterior

which agrees with the initial observation.

We pick target parameters θ^* at the center of the parameter space and execute the model with these parameters 100 times to account for trial-to-trial variations due to temporal noise. The mean of the observed decay constants is our target observation $\mathbf{x}^* = [\bar{\tau}^*] = 1.17 \pm 0.04$; the decay constant is in units of “compartments”.

We use a uniform distribution over all possible parameters as a prior distribution $p(\theta)$ and execute the SNPE algorithm to obtain an approximation of the posterior distribution $p(\theta | \mathbf{x}^*)$.

The correlation between the leak g_{leak} and the axial conductance g_{axial} is clearly visible in the approximated posterior, Figure 3C. The posterior distribution shows high densities for parameters θ which reproduced observations near the target observation during the grid search, compare contour lines in Figure 3A. For larger leak conductances g_{leak} the posterior probability decreases. This also agrees with the spread of the contour lines fitted to the grid search result.

In order to perform a posterior-predictive check (PPC), we draw samples $\{\theta_i\}$ from the posterior distribution, Figure 3C, configure our model with them and compare the observations $\{\mathbf{x}_i\}$ with the target observation \mathbf{x}^* . We measure a mean decay constant of $\bar{\tau} = 1.20 \pm 0.09$ which agrees within uncertainty with the target $\tau^* = 1.17 \pm 0.04$. Therefore, we conclude that the approximated posterior is in agreement with the target observation τ^* .

If we want to rediscover parameters which are closer to our original parameters θ^* , we need more informative observations. While the PSP heights show a similar decay for different sets of leak and axial conductance, Figure 3B, the absolute heights of the PSPs differ, Figure 3E. We can therefore use the PSPs heights which result from an input to the first compartment \mathbf{F} as a target observation $\mathbf{x}^* = \mathbf{F}^*$ to further constrain possible

parameters. Samples $\{\theta_i\}$ drawn from the posterior are now scattered around the original parameter θ^* in the parameter space and both parameters seem uncorrelated, Figure 3D; the Pearson correlation coefficient decreases from 0.93 to 0.06. The marginal distribution of the leak and axial conductance are bell-shaped and show a high density near the target parameter θ^* .

In order to validate the results we obtained in this section, we implemented a computer simulation in the simulation library Arbor (*Abi Akar et al.*, 2019). The topology of the parameter space as well as the shape of the approximated posteriors agree well between emulation and simulation, see Figure 9.

2.2 Multidimensional Parameter Space

In order to increase the problem complexity, we set the leak and axial conductance for each compartment and connection individually. For four compartments this results in a total of seven parameters.

As in the previous section we use a uniform prior and the PSP heights caused by an input to the first compartment as a target ($\mathbf{x}^* = \mathbf{F}^*$). We then execute the SNPE algorithm and draw samples from the approximated posterior $p(\theta | \mathbf{x}^*)$.

The marginal distribution of the sampled leak conductance in the first compartment g_{leak}^0 is bell-shaped and peaks near the target parameter, Figure 4A. The almost uniform distributions of the leak conductances in the other compartments indicate that they are not relevant for the chosen observation. In contrast, the marginal distribution of all axial conductances are bell-shaped with a high density around the original parameters. The distributions of the axial conductance become broader as we advance along the chain, suggesting that the influence on the observable weakens for axial resistances later in the chain.

We once again use a PPC to check if samples drawn from the approximated posterior $\{\theta_i\}$ reproduce the target observation. The mean difference between observations $\{\mathbf{H}_i\}$ obtained with these parameters and a target observation \mathbf{H}^* are displayed in Figure 4B. \mathbf{H} describes the observation of all PSP heights for inputs to different compartments and the target observation \mathbf{F}^* was extracted from \mathbf{H}^* , see Figure 2.

The mean of the PSP heights for an input to the first compartment (first column) is near the initial target values; the standard deviation is in the range of 1 to 2 σ^* where σ^* is the standard deviation of the measurements which were used to extract the target observation \mathbf{H}^* . A similar behavior can be seen if we only look at the response in the first compartment (first row), indicating that for these observations the leak conductance in the first compartment and the axial conductances are most relevant. For the other PSP height the mean is still in the two-sigma range of the initial target observation, but the standard deviation of the observations is significantly higher. This is expected since we did not use these PSP heights as an observation and the higher standard deviation can be attributed to the broad posterior distribution of the leak and axial conductance in later compartments.

Similar to the two-dimensional case, we can consider a higher-dimensional observation as a target to retrieve narrower posterior distributions. When we choose all PSP heights as a target ($\mathbf{x}^* = \mathbf{H}^*$) the posterior distribution becomes narrower, Figure 4A. Now the one-dimensional marginals of all parameters are bell-shaped. The marginals of the axial conductance show a narrower distribution than these of the leak conductance, indicating that the given observation is more sensitive to the axial conductance. The posterior distribution of the leak conductance in the first and last compartment show a similar confidence, while the distributions are broader for the two compartments within the chain.

The sharpening of the posterior distribution is also visible in the results of the PPC, Figure 4B. Here the standard deviation of the observations is now in the range of 1 to 2 σ^* for all PSP heights.

3 Discussion

We have shown that the sequential neural posterior estimation (SNPE) algorithm can be used to parameterize the analog neuromorphic BrainScaleS-2 (BSS-2) system. To be able to validate the approximated posteriors found by the SNPE algorithm, we selected a multi-compartmental model which takes the form of a chain of passive compartments. We chose the leak conductance as well as the axial conductance between compartments as parameters and observe how post-synaptic potentials (PSPs) propagate along the chain. This model allows us to easily change the dimensionality of the parameter space as well as the choice of observable and evaluate how this influences the approximated posteriors.

In all our experiments, we pick a set of target parameters, extract an observation with these parameters and then use the SNPE algorithm to approximate the posterior distribution of the parameters which reproduce this given observation.

As a first step, we considered a two-dimensional parameter space where we set all leak conductances and axial conductances to the same value. The low dimensionality of the parameter space allowed us to perform a grid search in a reasonable amount of time. The posterior approximation found with the SNPE algorithm agrees with the results from this grid search. In both cases we find a correlation between the leak and axial conductance if we look at the attenuation of PSPs; this agrees with theoretical expectations (*Fatt and Katz*, 1951; *Rall*, 1962). To be able to find such correlation is one of the advantages of a posterior approximation over traditional parameter search results which usually only yield a set of parameters which reproduce the given observation but do not illustrate the relation between different parameters.

When we chose a more informative observation, specifically the height of the PSPs which result from an input to the first compartment, the posterior distribution of the parameters narrows and the correlation between leak and axial conductance vanishes. We further show that the algorithm is capable of finding appropriate posterior approximations for several, random values of the target parameters. The approximations are even in agreement with the target parameters if they lie at the edges of the parameter space. This indicates that the algorithm is able to deal with the hard parameter limits which are dictated by the neuromorphic hardware.

Next, we increased the dimensionality of the parameter space by adjusting each leak and axial conductance individually; resulting in a seven-dimensional parameter space. We show that the marginal distributions of samples drawn from the posterior approximation have a high density around the target parameters. Furthermore, we perform posterior-predictive checks (PPCs) to confirm, that the parameters drawn from the approximated posterior produce emulation results which are in agreement with the target observation. As in the two-dimensional case, increasing the dimensionality of the observable leads to narrower posterior distributions.

Simulation which we performed in the simulation library Arbor show results which are comparable to the emulation results on BSS-2 (*Abi Akar et al.*, 2019). The topology of the two-dimensional parameter spaces agree well between simulation and emulation. Even though the approximated posteriors are narrower for the simulations, the overall shape resembles the shape of the posterior distributions found for emulations on

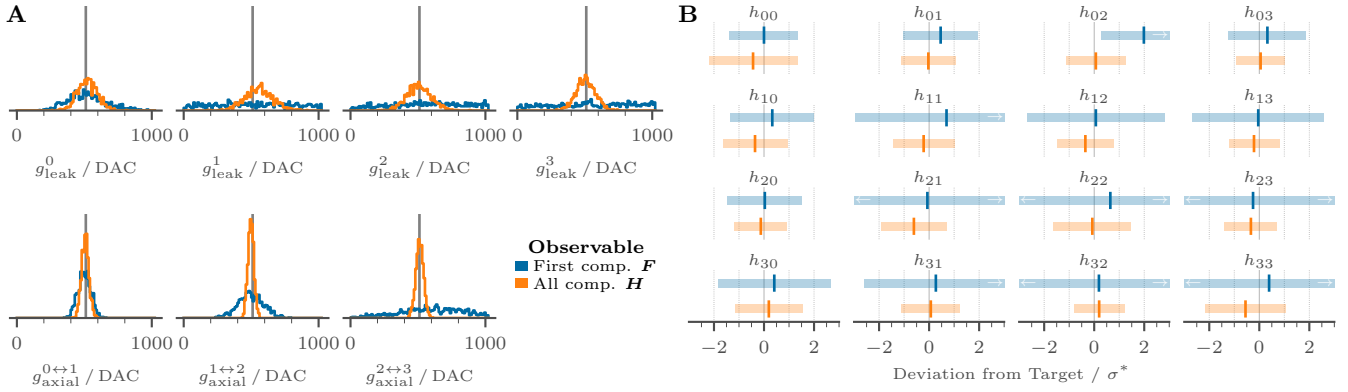


Figure 4: Results of the sequential neural posterior estimation for a compartment chain of 4 compartments and setting parameters individually for each compartment and connection between them. Emulations were performed on the neuromorphic BrainScaleS-2 system. **A** Histograms of 1000 parameters drawn from the approximated posterior. If we chose the heights \mathbf{F} of the post-synaptic potentials (PSPs) which result from an input to the first compartment as a target observation (blue), the distribution of the leak conductance in the first compartments is bell-shaped and peaks near the target parameter (dotted line). The leak conductance is roughly uniformly distributed in later compartments. The distributions of the axial conductance are bell-shaped and broaden for later compartments. Choosing all heights \mathbf{H} as a target (orange) leads to narrower distributions. All histograms are now bell-shaped with a peak near the target (dotted line). **B** Posterior-predictive check. The passive chain is configured with the parameters $\{\theta_i\}$ drawn in panel A and the PSP heights in all compartments $\{H_i\}$ are measured on the BrainScaleS-2 system. These PSP heights are compared to the observation \mathbf{H}^* which represents the measurement with the target parameters θ^* . The vertical lines show the mean deviation of the observations $\{H_i\}$ from this target \mathbf{H}^* while the horizontal bars illustrate the standard deviation of this deviation. As mentioned in the introduction, analog hardware is subject to temporal noise. Therefore, the target hardware was configured to the target parameters θ^* 100 times and the mean PSP heights were chosen as a target \mathbf{H}^* ; the deviation in this panel are scaled by the standard deviation σ^* of these 100 measurements (each height deviation h_{ij} is divided by the standard deviation of this height σ_{ij}^*). For all PSP heights the mean observation is within 1 to 2 standard deviations of the initial target. When a more informative observation \mathbf{H} is chosen, the standard deviations of the heights which do not include inputs or measurements in the first compartment more than halves.

BSS-2.

Our current results are limited to observations which were created by the model itself. Therefore, we can be certain, that model parameters exist which reproduce the given observation. In subsequent studies, we will use the SNPE algorithm to replicate observations which are provided by another model such as a numerical simulation or by physiological experiments. As seen in the grid search results, we dealt with a rather smooth parameter space, where the observations change gradually with the model parameters. In future, we will challenge the SNPE algorithm with somatic and dendritic spikes.

In summary, we show that the SNPE algorithm is suitable to find posterior approximations for parameters of the analog neuromorphic BSS-2 system. The algorithm is able to deal with the inherent trial-to-trial variations and the fixed parameter ranges of the BSS-2 system.

4 Methods

The experiments presented in this paper were emulated on the latest version of the BSS-2 system (Pehle et al., 2022; Billaudelle et al., 2022). We used the PyNN domain-specific language (Davison et al., 2009) to formulate the experiments and the BSS-2 OS to define and control the experiments (Müller et al., 2020).

4.1 Neuron Parameters

In order to ensure a similar behavior of the different compartments, the leak potential and the synaptic properties were calibrated. The synaptic time constant was calibrated to a value of 10 μ s. As can be extracted from Figure 3A, the decay constant varied in our experiments between 0.16 to 4.08 compartments. When varying the leak conductance g_{leak} over the full range specified in Figure 3, the membrane time constant $\tau_m = \frac{C_m}{g_{\text{leak}}}$ varies in the range of 12 μ s to 30 μ s.

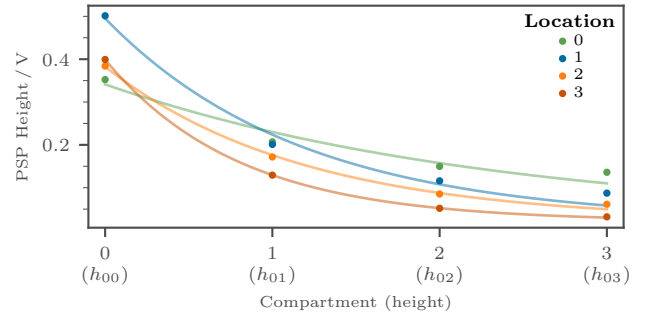


Figure 5: Exponential fit to the traces displayed in Figure 3B and Figure 3E. The heights of the post-synaptic potentials (PSPs) are extracted from the recorded membrane traces, compare Figure 2, and exponentials (solid lines) are fitted to the measurement points. The numbering is the same as in Figure 3. The x-axis label mark the compartment in which the height of the PSP was measured and in brackets the variable name as defined in Figure 2.

4.2 Predictive Posterior Check

We used PPCs for checking if an approximated posterior $p(\theta | \mathbf{x}^*)$ yields parameters θ which are in agreement with the original observation \mathbf{x}^* . As discussed in (Lueckmann et al., 2021) PPCs do not measure the similarity of the approximated to the true posterior and should just be used as a check rather than a metric. Nevertheless, we found that PPC were sensitive enough to highlight posterior approximations which did not agree with our expectation of the posterior based on the grid search results.

For all PPCs we drew 1000 random parameters $\{\theta_i\}$ from the approximated posterior $p(\theta | \mathbf{x}^*)$, emulated the chain model with these parameters on BSS-2 and recorded the observables $\{\mathbf{x}_i\}$. We evaluated how the hyperparameters of the SNPE algorithm influence the approximation success by comparing the mean Euclidean distance between these observations and the target observation \mathbf{x}^* .

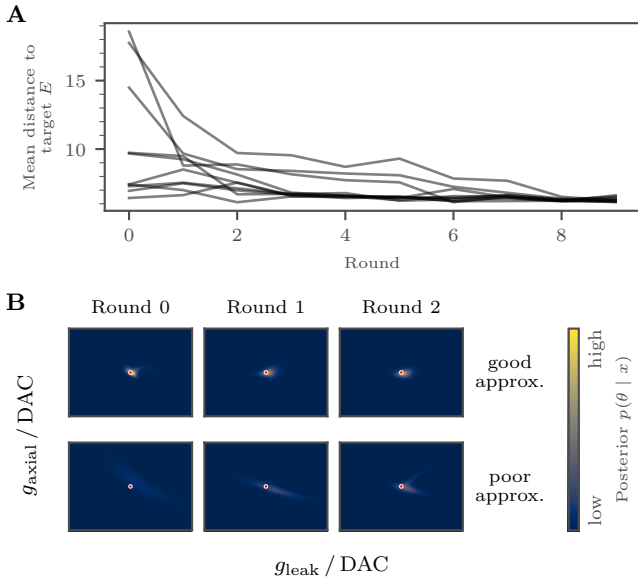


Figure 6: Evolution of the approximated posterior over several rounds of the sequential neural posterior estimation (SNPE) algorithm. Results are shown for emulations executed on the BrainScaleS-2 system. **A** Posterior-predictive check (PPC) for an emulation budget of 10 rounds with 50 emulations in each round (the PPC was executed with 1000 parameters sampled from the posteriors). The SNPE algorithm was executed 10 times with different seeds. For some executions of the SNPE algorithm, the approximated posterior in the first round poorly replicates observations which are similar to \mathbf{x}^* ; this is evident in a high mean distance E . In all displayed cases the SNPE algorithm is able to recover a meaningful posterior. **B** Examples for one case where SNPE algorithm is able to approximate a meaningful posterior and one case in which the algorithm fails to find a good approximation in the first three rounds. In both cases, the approximation in the first round does not agree with true posterior. In the top row, the algorithm is able to quickly recover from the poor approximation while in the bottom row more rounds are needed to obtain a meaningful approximation. The parameter ranges are the same as in Figure 3C.

4.3 Sequential Neural Posterior Estimator Algorithm

We use the SNPE algorithm proposed in (Greenberg et al., 2019) to find an approximation of the posterior distribution, compare Figure 1B. All our experiments were performed with the implementation provided in the `python` package `sbi`⁴ in version 0.21.0 (Tejero-Cantero et al., 2020).

We adjusted the number of simulations as well as the properties of the neural density estimator (NDE) and used PPCs to check how these hyperparameters influence the approximated posterior. For each set of hyperparameters we executed the SNPE algorithm ten times with different seeds. The seeds influence the initial weights as well as the parameters θ which are drawn from the prior in the first round. Different sets of hyperparameters shared the same seeds.

4.3.1 Number of Simulations and Rounds

For the two-dimensional parameter space and the decay constant τ as an observable, three times 50 emulations were sufficient to recover a posterior which is in agreement with the target observation.

When the observable is changed to the height of the PSPs which result from an input to the first compartment F , the SNPE algorithm failed to find a suitable approximation if the number of emulations was too low. This was due to a poor approximation in the first round from which the algorithm was not always able to recover, Figure 6. We observed that a higher number of emulations in the first round reduced the number of cases where the posterior was approximated poorly. Therefore,

⁴<https://github.com/mackelab/sbi>

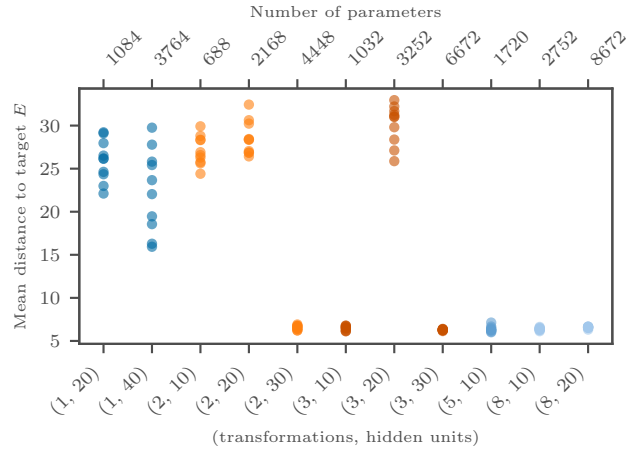


Figure 7: Influence of the parameterization of the neural density estimator (NDE) on the approximation of the posterior. We use masked autoregressive flows (MAFs) as NDEs. MAFs transform normal distributions in other distributions (Papamakarios et al., 2017). We use transformations which are made up of two blocks and change the number of hidden units which are used in each block (Gonçalves et al., 2020). Furthermore, we change the number of transformations which are chained together. As in Figure 6A we perform a posterior-predictive check and use the mean distance between these samples and the target observation \mathbf{x}^* . Again, we use the post-synaptic potential heights resulting from an input to the first compartment as an observable and repeat the sequential neural posterior estimation algorithm with 10 different seeds for each set of hyperparameters. At least two transformation are needed to recover a meaningful posterior. The number of experiments in which a meaningful posterior can be recovered seems to increase with the number of transformations. The total number of trainable parameters is not an indicator how well the NDE is able to approximate the true posterior.

we choose 500 emulations in the first round followed by ten rounds of 50 emulations for a two-dimensional parameter space with F as an observable.

4.3.2 Neural Density Estimator

Based on the results in (Lueckmann et al., 2021) we use masked autoregressive flows (MAFs) as NDEs (Papamakarios et al., 2017). MAFs transform normal distributions in other probability distributions. We used the values provided by the `sbi` package (Tejero-Cantero et al., 2020) as defaults; similar values have also been used in previous publications (Lueckmann et al., 2021; Gonçalves et al., 2020). Here the MAF is made up of five transformations which are chained together. Each of these transformation consists of two blocks with 50 hidden neuron per block. For more information see (Papamakarios et al., 2017, 2021).

In case of a two-dimensional parameter space and the decay constant τ as a target, Section 2.1, a single transformation with two blocks of ten hidden units each was sufficient. If we selected the heights which result from an input to the first compartment F as a target, a single transformation was not sufficient to recover a meaningful posterior, Figure 7. Starting from two transformations and 30 hidden units, the best value of the PPC were obtained. The only exception is the network with three transformations and 20 hidden units for which the algorithm could not recover from a poor approximation in the first round.

A MAF with one transformation and 50 is made up of 3764 trainable parameters and fails to approximate the true posterior. On the other hand a MAF with five transformations and 10 hidden units in each block offers just 1720 trainable parameters but is able to find approximations which agree with the target observation. We conclude, that a high number of transformations is more important for a good posterior approximation than a high number of trainable parameters. For the

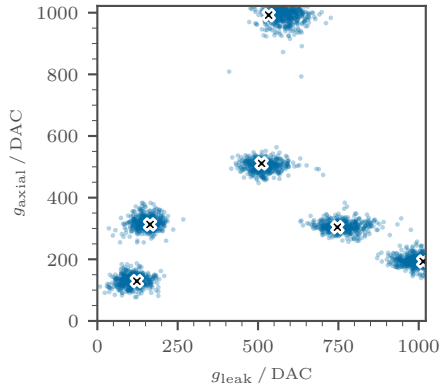


Figure 8: Posterior samples $\{\theta_j\}_i \sim p(\theta | \mathbf{x}_i^*)$ for different observations \mathbf{x}_i^* . We draw five random parameters θ_i from a uniform prior and one parameter at the center of the parameter space (marked by black crosses). The target observations $\{\mathbf{x}_i^*\}$ were obtained by emulating the model 100 times for each parameter on BrainScaleS-2 and taking the mean height of the post-synaptic potential obtained from an input to the first compartment, compare Figure 3D. As a posterior approximation we used the first round posterior obtained while executing the sequential neural posterior estimation algorithm in Section 2.1.2. The samples drawn from the approximated posterior (small dots) are in the vicinity of the parameters which were used to create the target observations (black crosses).

results reported in Figure 3D we used the NDE with five transformations, two blocks and ten hidden units.

4.4 Choice of the Target Parameters

We chose a target parameter θ^* at the center of the parameter space to measure target observations \mathbf{x}^* . For the experiment with the two-dimensional parameter space and the PSP heights for an input to the first compartment, we want to show that the approximated posterior is also appropriate for other choices of the target parameter θ^* . As mentioned in the introduction, the posterior estimation is amortized after the first round of SNPE and can therefore be used to infer parameters θ for any observation \mathbf{x} . We draw five random parameters $\{\theta_i^*\}$ from the uniform prior and emulate the model on BSS-2 with the given parameters to record observations $\{\mathbf{x}_i^*\}$. For each of these observations, we draw samples from the amortized posterior estimation $\theta \sim p(\theta | \mathbf{x}_i^*)$, Figure 8.

For each of the randomly selected observations \mathbf{x}_i^* the drawn samples cluster around the parameters which were used to obtain the given observation θ_i^* . Even if the target parameters are at the edge of the parameter space, the approximated posterior returns samples near these target parameters. Therefore, we conclude that the SNPE algorithm is suitable to find parameters for observations which were obtained for parameters at arbitrary locations in the parameter space and that our choice of target parameters θ^* at the center of the parameter space does not affect the generality of the reported results.

4.5 Simulations

We used the Arbor simulation library (version 0.8.1) to compare our results to computer simulations (Abi Akar et al., 2019). We simulated a chain with four compartments. The length of a single compartment was set to $l_{\text{comp}} = 1$ mm, its diameter to $d_{\text{comp}} = 4$ μm and its capacitance to $C = 125$ pF. While the length and diameter are chosen arbitrarily, the capacitance reflects the capacitance of the compartments used during the emulation on BSS-2. The range of the leak conductance g_{leak} is chosen such that the membrane time constant of the simulated neurons is in agreement with the emulated neurons on BSS-2. Similarly, the range of the axial conductance g_{axial} was chosen such that the axial conductance along a simulated compart-

ment is comparable to the conductance between compartments on BSS-2.

The chosen parameter ranges lead to a slightly higher decay conductance, compare Figure 9. Apart from that the behavior of the decay constant is in agreement with the emulations presented in Section 2.1.

The shapes of the approximated posteriors also agree with the results obtained for simulations on BSS-2. But due to the temporal noise on BSS-2, the approximated posterior distribution for the simulation are narrower than the approximation for BSS-2.

Contributions

J.K., J.S. and S.S. designed research; J.K. and R.S. performed research; J.K., J.S, R.S. and S.S. analyzed data; J.K. and S.S. wrote the paper; all authors edited the paper; E.M., J.K., R.S. and S.S contributed software; and J.S. designed the BrainScaleS-2 neuromorphic system.

Acknowledgments

We thank the lead of HBP’s FIPPA project Christian Tetzlaff for scientific input; A. Baumbach, S. Billaudelle, A. Grübl, J. Ilmberger, C. Mauch, C. Pehle, Y. Stradmann, P. Spilger and, J. Weis for their contributions to BSS-2; as well as all present and former members of the Electronic Vision(s) research group.

This work has received funding from the EU ([FP7/2007–2013], [H2020/2014–2020]) under grant agreements 604102 (HBP), 720270 (HBP SGA1), 785907 (HBP SGA2) and 945539 (HBP SGA3); the Deutsche Forschungsgemeinschaft (DFG, German Research Foundation) under Germany’s Excellence Strategy EXC 2181/1-390900948 (the Heidelberg STRUCTURES Excellence Cluster) as well as from the Manfred Stärk Foundation.

References

- Aamir, S. A., P. Müller, G. Kiene, L. Kriener, Y. Stradmann, A. Grübl, J. Schemmel, and K. Meier, A mixed-signal structured AdEx neuron for accelerated neuromorphic cores, *IEEE Transactions on Biomedical Circuits and Systems*, 12(5), 1027–1037, doi:10.1109/TBCAS.2018.2848203, 2018.
- Abi Akar, N., B. Cumming, V. Karakasis, A. Küsters, W. Klijn, A. Peyser, and S. Yates, Arbor—a morphologically-detailed neural network simulation library for contemporary high-performance computing architectures, in *2019 27th euromicro international conference on parallel, distributed and network-based processing (PDP)*, pp. 274–282, IEEE, 2019.
- Baker, R. E., J.-M. Peña, J. Jayamohan, and A. Jérusalem, Mechanistic models versus machine learning, a fight worth fighting for the biological community?, *Biol. Lett.*, 14(5), 20170,660, doi:10.1098/rsbl.2017.0660, 2018.
- Berger, T., M. E. Larkum, and H.-R. Lüscher, High I(h) channel density in the distal apical dendrite of layer V pyramidal cells increases bidirectional attenuation of EPSPs, *J. Neurophysiol.*, 85(2), 855–868, doi:10.1152/jn.2001.85.2.855, 2001.
- Billaudelle, S., J. Weis, P. Dauer, and J. Schemmel, An accurate and flexible analog emulation of AdEx neuron dynamics in silicon, *arXiv preprint*, doi:10.48550/arXiv.2209.09280, 2022.
- Brette, R., and W. Gerstner, Adaptive exponential integrate-and-fire model as an effective description of neuronal activity,

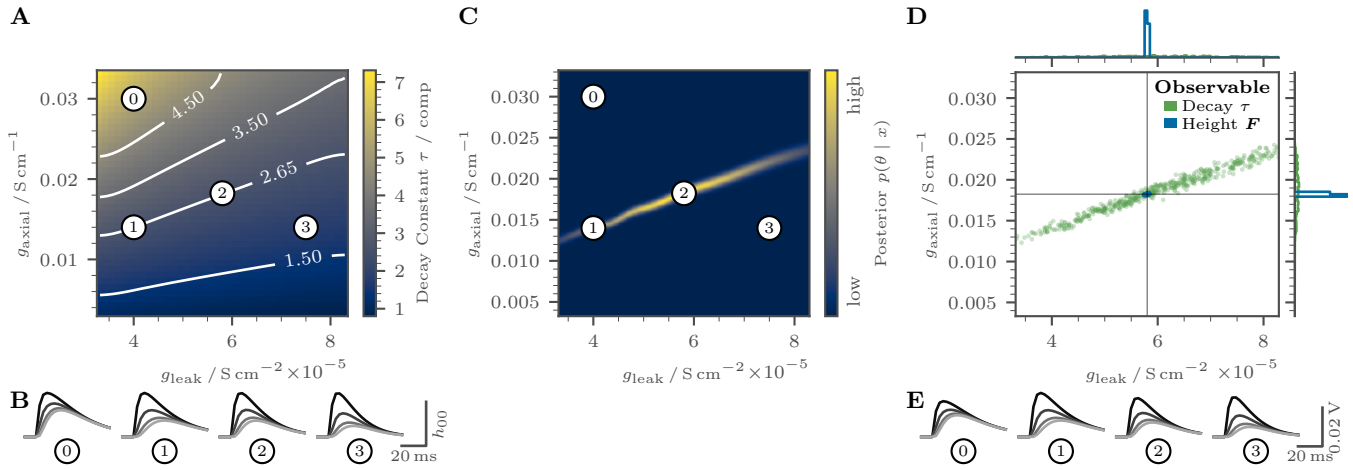


Figure 9: Propagation of post-synaptic potentials (PSPs) in a passive chain of four compartments simulated in Arbor. We performed the same experiments as in Figure 3 and we follow the structure of this figure. **A** Grid search of the decay constant τ . For the chosen parameter range the decay constant is slightly higher than on BSS-2. The dependency on the leak conductance g_{leak} and the axial conductance g_{axial} is comparable to Figure 3A. **B** Example traces recorded at different locations in the parameter space, compare panel A. The traces are scaled relative to the height in the first compartment h_{00} . **C** Posterior obtained with the sequential neural posterior estimation algorithm. While the shape of the approximated posterior is comparable to the one in Figure 3C, the approximated posterior for the simulations is narrower. **D** 500 random samples drawn from the approximated posteriors for two different types of observations. The distribution of the random samples is comparable to the results in Figure 3D, but in agreement with the narrower posterior in panel C, the distribution of the samples is more narrow. **E** Same traces as in panel B but shown on an absolute scale.

J. Neurophysiol., 94, 3637 – 3642, doi:10.1152/jn.00686.2005, 2005.

Cranmer, K., J. Brehmer, and G. Louppe, The frontier of simulation-based inference, *Proceedings of the National Academy of Sciences*, 117(48), 30,055–30,062, doi:10.1073/pnas.1912789117, 2020.

Davies, M., et al., Loihi: A neuromorphic manycore processor with on-chip learning, *IEEE Micro*, 38(1), 82–99, doi:10.1109/MM.2018.112130359, 2018.

Davison, A. P., D. Brüderle, J. Eppler, J. Kremkow, E. Müller, D. Pecevski, L. Perrinet, and P. Yger, PyNN: a common interface for neuronal network simulators, *Front. Neuroinform.*, 2(11), doi:10.3389/neuro.11.011.2008, 2009.

Deistler, M., P. J. Goncalves, and J. H. Macke, Truncated proposals for scalable and hassle-free simulation-based inference, *arXiv preprint*, doi:10.48550/arxiv.2210.04815, 2022.

Fatt, P., and B. Katz, An analysis of the end-plate potential recorded with an intra-cellular electrode, *The Journal of Physiology*, 115(3), 320–370, doi:10.1113/jphysiol.1951.sp004675, 1951.

Furber, S. B., D. R. Lester, L. A. Plana, J. D. Garside, E. Painkras, S. Temple, and A. D. Brown, Overview of the SpiNNaker system architecture, *IEEE Transactions on Computers*, 99(Preliminary), doi:10.1109/TC.2012.142, 2012.

Gonçalves, P. J., et al., Training deep neural density estimators to identify mechanistic models of neural dynamics, *eLife*, 9, doi:10.7554/eLife.56261, 2020.

Greenberg, D., M. Nonnenmacher, and J. Macke, Automatic posterior transformation for likelihood-free inference, in *Proceedings of the 36th International Conference on Machine Learning*, vol. 97, pp. 2404–2414, PMLR, 2019.

Hock, M., A. Hartel, J. Schemmel, and K. Meier, An analog dynamic memory array for neuromorphic hardware, in *Circuit Theory and Design (ECCTD), 2013 European Conference on*, pp. 1–4, doi:10.1109/ECCTD.2013.6662229, 2013.

Indiveri, G., et al., Neuromorphic silicon neuron circuits, *Frontiers in Neuroscience*, 5(0), doi:10.3389/fnins.2011.00073, 2011.

Kaiser, J., S. Billautelle, E. Müller, C. Tetzlaff, J. Schemmel, and S. Schmitt, Emulating dendritic computing paradigms on analog neuromorphic hardware, *Neuroscience*, 489, 290–300, doi:10.1016/j.neuroscience.2021.08.013, 2022.

Lueckmann, J.-M., P. Goncalves, G. Bassetto, K. Öcal, M. Nonnenmacher, and J. Macke, Flexible statistical inference for mechanistic models of neural dynamics, in *Advances in Neural Information Processing Systems*, vol. 30, 2017.

Lueckmann, J.-M., J. Boelts, D. Greenberg, P. Goncalves, and J. Macke, Benchmarking simulation-based inference, in *Proceedings of the 24th International Conference on Artificial Intelligence and Statistics (AISTATS)*, vol. 130, pp. 343–351, PMLR, 2021.

Mayr, C., S. Hoepfner, and S. Furber, Spinnaker 2: A 10 million core processor system for brain simulation and machine learning, *arXiv preprint arXiv:1911.02385*, 2019.

Müller, E., C. Mauch, P. Spilger, O. J. Breitwieser, J. Klähn, D. Stöckel, T. Wunderlich, and J. Schemmel, Extending BrainScaleS OS for BrainScaleS-2, *Tech. rep.*, Electronic Vision(s), Kirchhoff Institute for Physics, Heidelberg University, Germany, Heidelberg, Germany, doi:2003.13750, 2020.

Papamakarios, G., and I. Murray, Fast ϵ -free inference of simulation models with bayesian conditional density estimation, in *Advances in Neural Information Processing Systems*, vol. 29, pp. 1036–1044, Curran Associates Inc., 2016.

Papamakarios, G., T. Pavlakou, and I. Murray, Masked autoregressive flow for density estimation, in *Advances in Neural Information Processing Systems*, vol. 30, 2017.

Papamakarios, G., E. Nalisnick, D. J. Rezende, S. Mohamed, and B. Lakshminarayanan, Normalizing flows for probabilistic modeling and inference, *Journal of Machine Learning Research*, 22(57), 1–64, 2021.

- Pehle, C., et al., The BrainScaleS-2 accelerated neuromorphic system with hybrid plasticity, *Frontiers in Neuroscience*, 16, doi:10.3389/fnins.2022.795876, 2022.
- Rall, W., Electrophysiology of a dendritic neuron model, *Biophysical journal*, 2(2 Pt 2), 145, 1962.
- Sisson, S. A., Y. Fan, and M. Beaumont, *Handbook of approximate Bayesian computation*, CRC Press, 2018.
- Tejero-Cantero, A., J. Boelts, M. Deistler, J.-M. Lueckmann, C. Durkan, P. J. Gonçalves, D. S. Greenberg, and J. H. Macke, sbi: A toolkit for simulation-based inference, *Journal of Open Source Software*, 5(52), 2505, doi:10.21105/joss.02505, 2020.
- Van Geit, W., E. De Schutter, and P. Achard, Automated neuron model optimization techniques: a review, *Biol. Cybern.*, 99(4), 241–251, doi:10.1007/s00422-008-0257-6, 2008.
- Vanier, M. C., and J. M. Bower, A comparative survey of automated parameter-search methods for compartmental neural models, *J Comput Neurosci*, 7(2), 149–171, doi:10.1023/a:1008972005316, 1999.
- Wunderlich, T., et al., Demonstrating advantages of neuromorphic computation: A pilot study, *Frontiers in Neuroscience*, 13, 260, doi:10.3389/fnins.2019.00260, 2019.